BEAMLINE DESIGN AND DIAGNOSTICS FOR STRONG X-Y COUPLED BEAMS USING A ROTATING QUADRUPOLE*

H. Iinuma†, Ibaraki University, Ibaraki, Japan
K. Furukawa, H. Nakayama, S. Ohsawa, N. Saito, K. Sasaki,
High Energy Accelerator Research Organization, Tsukuba, Japan
M. A. Rehman, Institute of High Energy Physics, Beijing, China
R. Matsushita, The University of Tokyo, Tokyo, Japan

Abstract

To measure spin precession in ultra-precise magnetic fields, we are developing a beam injection technique based on a three-dimensional spiral trajectory. As a representative case, the transverse phase-space requirements for injecting a 300 MeV/c muon beam into a solenoid-type storage magnet (central field: 3 T, local field uniformity controlled below 0.1 ppm using medical-MRI technology) were previously reported at IPAC25/WEPM029. In this presentation, we introduce a beam phase-space design concept using a quadrupole magnet that can be rotated by an arbitrary angle around the beam (Z) axis, and we show an example transport line that successfully achieves the required X–Y coupling. We further discuss a beam-diagnostics scheme employing the rotating quadrupole to determine a full 4×4 σ-matrix. Promising operational results on the control of X–Y coupled beams—obtained from the demonstration experiments conducted between 2014 and 2024—will also be presented, indicating that the approach is moving in the expected and desirable direction.

INTRODUCTION

Conventional beamline design for large-scale accelerators has been developed under the free-space approximation, where external magnetic fields can be neglected. In contrast, beam injection into compact storage rings as in shown Fig. 1 involves strong field gradients, requiring a formulation based on canonical variables including the vector potential. Although the theoretical framework is well established, it has not been systematically developed into practical design principles applicable to real devices. In this study, we present a design framework for beam transport in strong-field environments, providing a basis for stable and precise beam control.

As a representative example, we consider beam control in a solenoidal storage magnet, where fringe fields play an essential role in shaping the beam dynamics. In this study, we develop a canonical beam transport framework including external magnetic fields and connect it to practical correction magnet design. The objective is to preserve phase-space consistency and demonstrate the effectiveness of the approach.

The beam is prepared with strong X–Y correlations, as shown in Fig. 2, to match the phase-space requirements for injection into the solenoidal magnetic field. This configuration has been described in detail in Refs. [1–3].

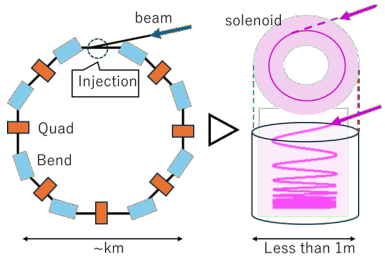

Figure 1: Concept of beam injection into a solenoidal storage magnet. A compact system replaces a large-scale beamline using a spiral trajectory.

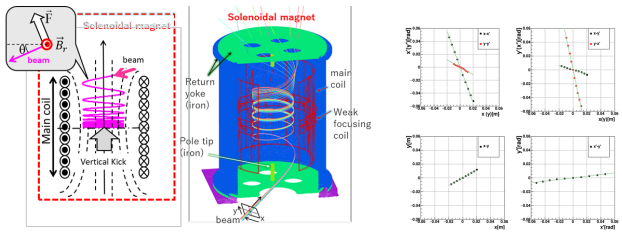

Figure 2: Beam control in a solenoidal storage magnet with fringe fields and correction coils. The beam dynamics is shaped by external magnetic fields.

In this study, we develop a canonical beam transport framework including external magnetic fields and connect it to practical correction magnet design. The objective is to preserve phase-space consistency and demonstrate the effectiveness of the approach.

CANONICAL BEAM DYNAMICS WITH VECTOR POTENTIAL

Beam dynamics is formulated in canonical coordinates including the vector potential, where the canonical angular momentum plays a central role. This framework enables a unified treatment of covariance matrices and eigen-emittances.

Left picture of Fig. 3 shows single-particle tracking of 20 trajectories inside the solenoidal storage magnet. Right side of Fig. 3 shows the particle momentum as a function of the solenoid axis (vertical). The canonical angular momentum is conserved within numerical precision, while the conservation law is violated if the vector potential term qRA_ϕ is not included.

* Work supported by by JSPS KAKENHI Grant Nos. 26287055, 19H00673, 22K14061, and 23KJ0590.
† hiromi.iinuma.spin@vc.ibaraki.ac.jp

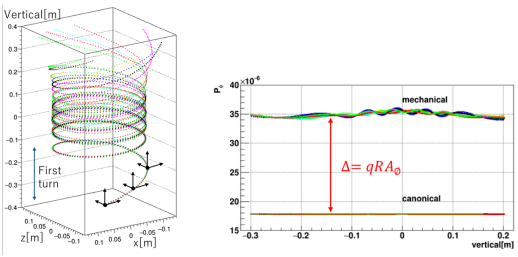

Figure 3: Single-particle tracking and angular momentum along the solenoid axis. The canonical angular momentum is conserved, unlike the mechanical one.

Conservation of Eigen Emittance

Having confirmed the validity of the single-particle tracking, we extend the discussion to beam dynamics. The beam is described by the covariance matrix Σ defined around slice points along the reference trajectory. The phase-space vector of the j^{th} particle at slice i^{th} is given by

$$\vec{q}_j = (\Delta x, \Delta p_x, \Delta y, \Delta p_y, \Delta z, \Delta p_z)^T, \quad (1)$$

and the ensemble of n particles is represented by a $6 \times n$ matrix X_i. Σ matrix at i^{th} is then,

$$\Sigma_i = X_i X_i^T. \quad (2)$$

The eigen-emittances are obtained from the symplectic eigenvalues of the covariance matrix, given by the eigenvalues of $J\Sigma$, where J is the standard symplectic matrix. The eigen-emittances ϵ_k are defined from the eigenvalues of $J\Sigma$, which appear in conjugate pairs $\pm i\epsilon_k$, where $k = 1, 2, 3$.

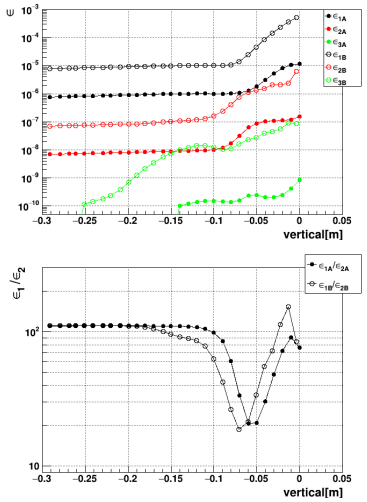

Figure 4: Eigen-emittances and their ratios along the reference trajectory. The eigen-emittances are approximately preserved over a wide region.

The eigen-emittances and their ratios are shown in Fig. 4 (left and right). The three eigen-emittances are approximately preserved over a wide region along the reference trajectory, although gradual deviations appear as the beam approaches the stronger fringe-field region. In particular, the larger eigen-emittance components remain relatively stable in the upstream region, while the smaller component shows stronger sensitivity to the magnetic-field structure and to the numerical conditions used in the slice-based evaluation. The ratios of the eigen-emittances in Fig. 4 (right) indicate that the relative mode structure is maintained over most of the transport region, whereas noticeable distortions appear near the region where the beam size increases and the field distribution becomes less favorable for an accurate covariance-matrix evaluation. These results suggest that the apparent variation of the eigen-emittances is governed not only by the beam evolution itself but also by the combined effect of beam expansion and magnetic-field profile.

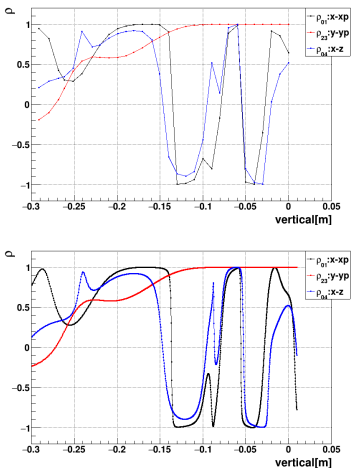

Figure 5: Correlation coefficients ρ derived from the covariance matrix. The phase-space structure evolves dynamically along the trajectory.

The correlation coefficients ρ are shown in Fig. 5 (left and right). Here, ρ is introduced as a normalized measure of phase-space correlation derived from the covariance matrix. The results show that the dominant correlations evolve systematically along the trajectory, reflecting the redistribution of phase-space structure under the external magnetic field. The overall trends are consistent between the fine-slice and coarse-slice evaluations, while the coarse-slice results exhibit a more segmented behavior due to the reduced spatial resolution. In particular, the evolution of ρ_{01}, ρ_{23}, and ρ_{04} demonstrates that the beam does not preserve a fixed pairwise correlation pattern, but instead undergoes a continuous reorganization of its phase-space structure. This behavior is consistent with the dynamical mode change of the Σ-matrix.

Beam Transport Matrices and Symplecticity

Beam transport matrices are evaluated from the covariance matrices at different locations. The symplecticity of the transport is assessed using the condition

$$X_{i+1} = MX_i + C \quad (3)$$

where M is a 6×6 matrix and C is a 6×1 phase-space offset vector as in Eq. (3).

The deviation from symplecticity is quantified by

$$\Delta M = M^T J M - J, \quad (4)$$

while the affine contribution is evaluated separately using the norm of the offset vector $\Delta\ C$. These quantities are compared to distinguish the effects of linear transport and affine offsets.

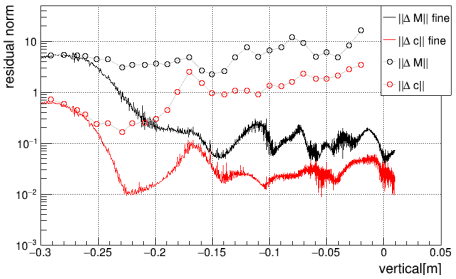

Figure 6: Residual norms of $\|\Delta\ M\|$ and $\|\Delta\ c\|$ long the trajectory. The symplecticity deviation dominates over the affine contribution.

Figure 6 shows the residual norms of $\|\Delta\ M\|$ and $\|\Delta\ C\|$ along the reference trajectory. The affine contribution is systematically smaller than the symplecticity deviation, indicating that the observed non-symplectic behavior originates primarily from the linear transport. While both fine-slice and coarse-slice evaluations show consistent trends, the coarse-slice results exhibit larger deviations, reflecting the sensitivity of the reconstruction to slice resolution.

To demonstrate the beam injection principles described above, we carried out systematic experimental studies over approximately ten years, from 2014 to 2024. The next section provides an overview of these demonstration experiments.

DEMONSTRAION EXPERIMENT

Figure 7 shows the beamline used to transport an 80 keV electron beam to the solenoidal storage magnet. Three rotating quadrupole magnets are employed to produce the beam conditions required for injection into the solenoidal field. Beam profile monitors are installed along the beamline to measure the transverse beam distribution. Details of the setup are given elsewhere [4].

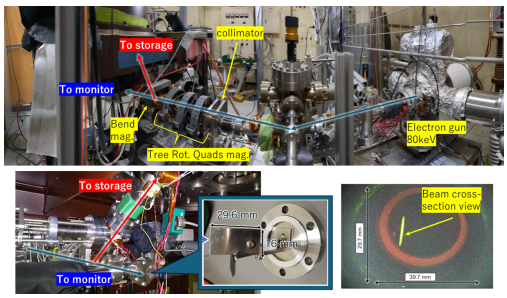

Figure 7: Experimental beamline for transporting an 80 keV electron beam. Rotating quadrupoles and monitors are used for beam shaping and diagnostics.

Figure 8 shows the solenoidal magnet and the correction coils used to generate a weak focusing field. The measured magnetic fields are in good agreement with OPERA-3D calculations. The balance between the main coil and correction coils allows flexible control of the weak focusing strength.

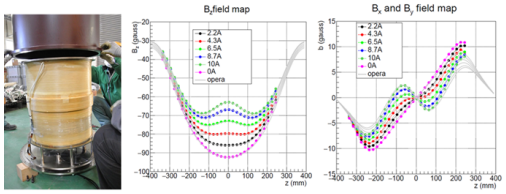

Figure 8: Solenoidal magnet and correction coils with measured and simulated fields. The weak focusing strength is controlled by balancing the coils.

Figure 9 shows the injection results for the rotating quadrupole settings listed in Table 1. The beam inside the storage magnet is visualized via ionization light in nitrogen gas using a wide-angle, high-sensitivity camera, enabling semi-online tuning of the vertical beam distribution and rotation center. Stable trajectories are obtained for multiple parameter sets, indicating that multiple phase-space solutions are compatible with successful injection. This implies that the transport connecting the Σ-matrix at the injection point to that in the storage region is not unique. Further details will be reported elsewhere.

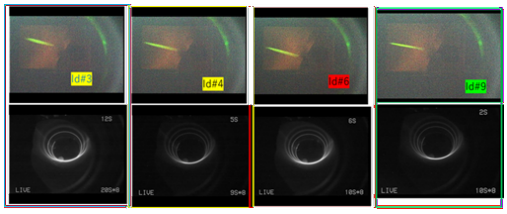

Figure 9: Beam images inside the storage region for different tuning conditions. Multiple phase-space solutions enable stable beam injection.

Table 1: Rotating quadrupole settings used for beam injection, where the three quadrupoles are labeled Q1 to Q3 from left to right.

Data No	Angles [°]	K [T/m]
3	0, 15, 45	-1.02, -89.22, 16.24
4	0, 15, 45	-5.99, -52,68, 10.05
6	0, 15, 45	-22.23, -70.95, 22.23
9	-20, 25, -45	-26.29, -72.98, 10.05

CONCLUSION

We presented a beam transport framework based on canonical coordinates including the vector potential. The eigen-emittances are approximately preserved even in non-ideal transport conditions, providing a robust description beyond conventional symplectic assumptions. The experimental results demonstrate that stable beam injection can be achieved with multiple configurations, indicating non-unique phase-space solutions. Beam storage using a kicker is beyond the scope of this paper and is discussed in Refs. [5, 6]. The preservation of eigen-emittances along the kicker trajectory is also addressed in Ref. [7].

REFERENCES

[1] H. Iinuma *et al.*, "Results from validation experiment for three-dimensional spiral beam injection scheme", in *Proc. IPAC'25*, Taipei, Taiwan, Jun. 2025, pp. 2894-2897. doi:10.18429/JACoW-IPAC2025-THPM099

[2] H. Iinuma *et al.*, "Trajectory design for passing through solenoid magnet fringe field and method for adjusting its strongly X-Y coupled phase space for three-dimensional spiral beam injection", in *Proc. IPAC'25*, Taipei, Taiwan, Jun. 2025, pp. 2020-2023. doi:10.18429/JACoW-IPAC2025-WEPM029

[3] H. Iinuma *et al.*, "Three-dimensional spiral injection scheme for the g2/EDM experiment at J-PARC", *Nucl. Instrum. Methods Phys. Res. A*, vol. 832, pp. 51-62, 2016. doi:10.1016/j.nima.2016.05.126

[4] H. Iinuma, R. Matsushita, M. A. Rehman, H. Nakayama, S. Ohsawa, and K. Furukawa "Three-dimensional spiral beam injection: Design principles and experimental verification", arXiv:2602.05518 [physics.acc-ph]. doi:10.48550/arXiv.2602.05518

[5] R. Matsushita *et al.*, "Results of demonstration experiment of three-dimensional spiral injection scheme for ultra-compact storage rings", presented at the 17th Int. Part. Accel. Conf. (IPAC'26), Deauville, France, May 2026 paper MOP6651, this conference.

[6] R. Matsushita *et al.*, "First experimental demonstration of beam storage by three-dimensional spiral injection scheme for ultra-compact storage rings", accepted by Phys. Rev. Lett., May 21, 2026. doi:10.1103/8nxx-srgz

[7] H. Iinuma *et al.*, "Study on evaluation method for transient response of conductor surface to large pulse current", presented at the 17th Int. Part. Accel. Conf. (IPAC'26), Deauville, France, May 2026 paper THP5621, this conference.